Computer-guided alignment II : Optical system alignment using differential wavefront sampling

Hanshin Lee[1, 3], **Gavin B. Dalton**[1, 2], **Ian A. J. Tosh**[2], **Sug-Whan Kim**[3]

[1]*Astrophysics sub-department, Department of Physics, University of Oxford, Oxford, UK*
[2]*Space Science and Technology Department, Rutherford Appleton Laboratory, Oxon, UK*
[3]*Space Optics Laboratory, Department of Astronomy, Yonsei University, Seoul, Korea*

hlee@astro.ox.ac.uk

Abstract: We present a differential wavefront sampling method for the efficient alignment of centred optical systems. Using the inter-element effects reported in our previous study, this method generates a linear symmetric matrix that relates the optical wavefront to misalignments within the system. The solution vector of this matrix equation provides a unique description of decentre and tilt misalignments of the system. We give a comparison of this approach to the existing method in the first case study and then illustrate characteristics of the new approach using the subsequent four case studies and Monte-Carlo alignment simulations. The results reveal superiority of the method over the existing one in misalignment estimation accuracy and demonstrate the practical feasibility and robustness.

OCIS codes: (220.1140) Alignment; (220.4840) Optical testing.

References and links

1. R. V. Shack and K. Thompson, "Influence of alignment errors of a telescope system on its aberration field," in *Optical alignment*, R. M. Shagam and W. C. Sweatt, eds., Proc. SPIE **251**, 146-153 (1980)
2. B. McLeod, "Collimation of Fast Wide-Field Telescopes," PASP **108**, 217-219 (1996).
3. R. N. Wilson and B. Delabre, "Concerning the Alignment of Modern Telescopes: Theory, Practice, and Tolerance Illustrated by the ESO NTT," PASP **109**, 53-60 (1997).
4. L. Noethe and S. Guisard, "Analytic expressions for field astigmatism in decentered two mirror telescopes and application to the collimation of the ESO VLT," A&A Supp. **144**, 157-167 (2000).
5. W. Sutherland, *Alignment and Number of Wavefront Sensors for VISTA*, VIS-TRE-ATC-00112-0012 (Technical report, Astronomy Technology Center, UK, 2001).
6. S. Kim, H.-S. Yang, Y.-W. Lee, and S.-W. Kim, "Merit function regression method for efficient alignment control of two-mirror optical systems," Opt. Express **15**, 5059-5068 (2007)
7. H. J. Jeong, G. N. Lawrence, and K. B. Nahm, "Auto-alignment of a three mirror off-axis telescope by reverse optimization and end-to-end aberration measurements," in *Current Developments in Optical Engineering II*, R. E. Fischer and W. J. Smith, eds., Proc. SPIE 818, 419-430 (1987)
8. M. A. Lundgren and W. L. Wolfe, "Alignment of a three-mirror off-axis telescope by reverse optimization," Opt. Eng. **30**, 307-311 (1991)
9. H. Chapman and D. Sweeney, "Rigorous method for compensation selection and alignment of microlithographic optical systems," in *Emerging Lithographic Technology*, Y. Vladimirsky, eds., Proc. SPIE **3331**, 102-113 (1998).
10. H. Lee, "Amon-Ra system alignment," in *Novel space optical instrument for deep space earth albedo monitoring*, 250-289 (Master thesis, Yonsei University, 2005).
11. H. Lee, G. B. Dalton, I. A. J. Tosh, and S.-W Kim, "Computer-guided alignment I : Phase and amplitude modulation of the alignment-influenced wavefront," Opt. Express **15**, 3127-3139 (2007)
12. G. B. Arfken and H. Weber, *Mathematical Methods for Physicist* 4th ed., (Academic press, London, 1996).
13. A. Malvick and E. Pearson, "Theoretical elastic deformations of a 4-m diameter optical mirror using dynamic relaxation," Appl. Opt. **7**, 1207-1212 (1968).
14. R. Tyson and B. W. Frazier, *Field Guide to Adaptive Optics*, (SPIE, Washington, 2004).

#87062 - $15.00 USD Received 30 Aug 2007; revised 24 Oct 2007; accepted 25 Oct 2007; published 6 Nov 2007

15. Private communication (Kevin Middleton, Oxford, 2007).
16. E. P. Goodwin and J. C. Wyant, *Field Guide to Interferometric Optical Testing*, (SPIE, Washington, 2004).
17. A. E. Bryson, *Applied Linear Optimal Control*, (Cambridge University Press, Cambridge, 2002)
18. A. Doucet, S. Godsill and C. Andrieu, "On sequential Monte Carlo sampling methods for Bayesian filtering," Statistics and computing **10**, 197-208 (2000)

1. Introduction

A measurement of the optical wavefront provides quantitative information of the physical state of an optical system. The alignment state, being one of those physical states, contains position and orientation information of the individual optical elements in a system and describes how they are aligned relative to each other. The influence of the alignment state on the system wavefront has been studied in terms of the field behaviour of a system in response to a given alignment state [1]. This led to an alignment state estimation method using multi-field wavefront samplings (MFWS hereafter). MFWS requires a set of linear field astigmatism measurements sampled at as many known fields as, at least, the number of unknown alignment parameters. It then establishes a set of equations relating the measured linear field astigmatism to the alignment state of individual optical elements. The alignment state is estimated either by solving the linear approximation form of the equations or by using non-linear optimisation methods. This method has been extensively used for studying the single-element alignment problem, e.g. the secondary mirror alignment in a two-mirror telescope system [2, 3, 4, 5, 6].

In parallel, various methods have been proposed for the optical alignment of some complex systems [7, 8, 9, 10]. These systems exhibit the multi-component alignment problem where MFWS finds an issue with the reliability of its state estimation. In particular, we have often witnessed this issue appearing evidently when the directional alignment parameters, i.e. decentres and tilts, of several elements are estimated simultaneously. This could be caused by intrinsic degeneracy and/or non-linear nature of the multi-element optical alignment which increase the probability that optimisation techniques stall in local minima or plateaux in solution space. This probability can be aggravated when other opto-mechanical state parameters need to be considered in addition to the alignment state. It is therefore desirable that wavefront-based alignment tools should be able to estimate the alignment state in a manner insensitive to such degeneracy and non-linear couplings between some, if not all, alignment state parameters. Such an approach could have important implications to many problems requiring accurate alignment state estimations and yet, to our best knowledge, has not been rigorously investigated.

Therefore, we propose an alignment state estimation method called differential wavefront sampling (DWS hereafter) which utilises the inter-element alignment effects reported in [11]. In Section 2, we compare DWS to MFWS in terms of their intrinsic characteristics. We then theoretically investigate the effects of measurement and control uncertainties and of surface deformations to the performance of DWS. The practical feasibility of DWS are then illustrated by case studies and Monte-Carlo simulations in Section 3, where we also discuss implications for practical alignment procedures.

2. DWS for alignment state estimation

The system wavefront (Φ) can be expressed as a linear sum of the nominal wavefront (Φ_0) and other additional wavefront contributions.

$$\Phi = \Phi_0 + \Phi_A + \Phi_D + \Phi_C + \Phi_R + \Phi_S \quad (1)$$

Φ_A and Φ_D are from misalignment and surface deformation, respectively. These two can couple with each other to generate a coupled variation (Φ_C). In addition, we may have random (Φ_R) and/or systematic (Φ_S) uncertainties, but we assume here that Φ_S can be calibrated ($\Phi_S = 0$).

#87062 - $15.00 USD Received 30 Aug 2007; revised 24 Oct 2007; accepted 25 Oct 2007; published 6 Nov 2007

In our previous study, we found that Φ_A contains significant non-linear couplings between alignment parameters [11]. These can lead to unreliable estimates of the alignment state using existing methods. The presence of Φ_D and Φ_C tends to complicate this situation even further. Therefore, it is desirable to have information that can be used to eliminate these couplings and for such information we propose the differential wavefront as described in Section 2.1.

2.1. Differential Wavefront and MFWS

The differential wavefront is defined as the wavefront differentiated with respect to any of the physical state parameters at a given state of a system. For the purposes of our study, we may express the derivative of the wavefront with respect to the alignment state of the i-th element ($\mathbf{u}_i$) as a series expansion as,

$$\frac{\partial \Phi_A}{\partial \mathbf{u}_i} = L_i^{(1)} + \sum_{j=0}^{M} (1+\delta_{ij})\, L_{ij}^{(2)} \cdot \mathbf{u}_j + \cdots \tag{2}$$

Here $\mathbf{u}_i$ includes linear misalignments in x- and y-axis (dx_i, dy_i), angular misalignments about x- and y-axis ($d\theta_i, d\phi_i$), and an axial misalignment in z-axis (dz_i). M is the number of elements in the system and $L^{(m)}$ is the alignment influence function of order *m* [11].

In Eq. 2, the first and the second order terms are of great importance because they generate coma and astigmatism respectively. However, the second order term is more important as it contains the alignment state vector and thus enables one to relate the alignment state to the optical wavefront.

MFWS already uses the concept of the differential wavefront, in that it forms a relation between a set of linear field astigmatism samples and the system alignment state. This relation resembles the second term in Eq. 2. To study MFWS a little further, consider a collimated test beam and a three-element system ($M = 3$) where only the second element is mis-aligned. We replace Φ_A by its 0° linear field astigmatism expressed in fringe Zernike polynomials, $Z_{5,L}$. This term is the characteristic component of $L_{i,j}^{(2)}$ in Eq. 2 and depends only on the directional alignment state parameters, i.e. decentre and tilt, of optical elements and lateral field positions of the source. This leaves four unknown alignment state parameters, $\mathbf{u}_2 = (dx_2, dy_2, d\theta_2, d\phi_2)$. Using $Z_{5,L}$ sampled at four fields, we construct the relation between the linear field-astigmatism and misalignment as,

$$\mathbf{Z}_{5,L} \;=\; \mathbf{M}_{5,M_2}\,\mathbf{u}_2 \;=\; \left(\mathbf{F}_5\,\mathbf{L}_{5,M_2}\right)\,\mathbf{u}_2 \tag{3}$$

where $\mathbf{Z}_{5,L}$=$\{Z_{5,L}^{(i)} : i=1, \cdots, 4\}^T$, $\mathbf{F}_5$=$\{d\mathbf{P}, d\mathbf{T}, d\mathbf{T}, d\mathbf{P}\}$, and $\mathbf{L}_{5,M_2}$=diag$\{L_{\phi_{0,x_2}}, L_{\theta_{0,y_2}}, L_{\theta_{0,\theta_2}}, L_{\phi_{0,\phi_2}}\}$ where $d\mathbf{P}$=$\{d\phi_0^{(i)} : i=1, \cdots, 4\}^T$, $d\mathbf{T}$=$\{d\theta_0^{(i)} : i=1, \cdots, 4\}^T$, and 'i' is the field index.

It is interesting that the influence matrix ($\mathbf{M}_{5,M_2}$) can be divided into two sub-matrices, one with a collection of field angles ($\mathbf{F}_5$) and the other with the influence coefficients ($\mathbf{L}_{5,M_2}$). It is obvious that $\mathbf{F}_5$ is a rank-2 matrix according to the matrix rank definition [12]. To uniquely determine $\mathbf{u}_2$ in Eq. 3, more equations are needed and we may use $Z_{6,L}$, the 45° linear field astigmatism, sampled at the same fields to provide four additional equations. We then combine the equations for $Z_{6,L}$ with Eq. 3 such that the resultant equation becomes Eq. 4 below.

$$\begin{bmatrix} \mathbf{Z}_{5,L} \\ \mathbf{Z}_{6,L} \end{bmatrix} = \left(\begin{bmatrix} \mathbf{F}_5, & \mathbf{0} \\ \mathbf{0}\ , & \mathbf{F}_6 \end{bmatrix} \begin{bmatrix} \mathbf{L}_{5,M_2} \\ \mathbf{L}_{6,M_2} \end{bmatrix} \right) \mathbf{u}_2 \tag{4}$$

where $\mathbf{Z}_{6,L}$=$\{Z_{6,L}^{(i)} : i=1, \cdots, 4\}^T$, $\mathbf{F}_6$=$\{d\mathbf{T}, d\mathbf{P}, d\mathbf{P}, d\mathbf{T}\}$, and $\mathbf{L}_{6,M_2}$=diag$\{L_{\theta_{0,x_2}}, L_{\phi_{0,y_2}}, L_{\phi_{0,\theta_2}}, L_{\theta_{0,\phi_2}}\}$. The new matrix with $\mathbf{F}_5$ and $\mathbf{F}_6$ is now rank-4 and thus $\mathbf{u}_2$ can be determined uniquely.

Let us suppose further that the third element in the system is also misaligned. We now need four more field samples of wavefront, eight samples in total, in which case we have

#87062 - $15.00 USD Received 30 Aug 2007; revised 24 Oct 2007; accepted 25 Oct 2007; published 6 Nov 2007

$$\begin{bmatrix} \mathbf{Z}'_{5,\mathrm{L}} \\ \mathbf{Z}'_{6,\mathrm{L}} \end{bmatrix} = \left(\begin{bmatrix} \mathbf{F}'_5, & \mathbf{0} \\ \mathbf{0}, & \mathbf{F}'_6 \end{bmatrix} \begin{bmatrix} \mathbf{L}_{5,\mathrm{M}_2}, & \mathbf{0} \\ \mathbf{0}, & \mathbf{L}_{5,\mathrm{M}_3} \\ \mathbf{L}_{6,\mathrm{M}_2}, & \mathbf{0} \\ \mathbf{0}, & \mathbf{L}_{6,\mathrm{M}_3} \end{bmatrix} \right) \begin{bmatrix} \mathbf{u}_2 \\ \mathbf{u}_3 \end{bmatrix} \tag{5}$$

where the aberration is given by $\mathbf{Z}'_{5,\mathrm{L}} = \{\mathrm{Z}^{(\mathrm{i})}_{5,\mathrm{L}} : \mathrm{i} = 1, \cdots, 8\}^{\mathrm{T}}$ and $\mathbf{Z}'_{6,\mathrm{L}} = \{\mathrm{Z}^{(\mathrm{i})}_{6,\mathrm{L}} : \mathrm{i} = 1, \cdots, 8\}^{\mathrm{T}}$, and the field matrices are $\mathbf{F}'_5 = [\mathbf{F}_5, \mathbf{F}_5]$ and $\mathbf{F}'_6 = [\mathbf{F}_6, \mathbf{F}_6]$ with $\mathrm{d}\mathbf{P} = \{\mathrm{d}\phi^{(\mathrm{i})}_0 : \mathrm{i} = 1, \cdots, 8\}^{\mathrm{T}}$ and $\mathrm{d}\mathbf{T} = \{\mathrm{d}\theta^{(\mathrm{i})}_0 : \mathrm{i} = 1, \cdots, 8\}^{\mathrm{T}}$. The field matrix in Eq. 5 is still rank-4 even though we added four more field samples in attempting to uniquely determine 8 unknowns. This means that Eq. 5 yields a degenerate solution that tends to give inaccurate alignment state of the system. Therefore, we expect that this approach would be limited in use to a single component alignment state estimation due to the intrinsic rank-deficiency. It is true that, in a typical centred system, the linear misalignment influence dominates over other higher-order effects. Thus it is unlikely that the inclusion of higher-order terms would make a significant difference to the intrinsic rank-deficiency.

We may use the first-order coma equations to provide additional constraints, however, one should note that coma associated with linear misalignment is constant over the field plane and thus effectively provides only two additional equations. In this case, one may be able to determine up to six unknown alignment parameters, for example six angular misalignment parameters in a three-element system, provided that the decentre misalignments are already known.

2.2. DWS

We now consider the same configuration as used first in Section 2.1, but with the test beam fixed in the centre field. We deliberately perturb the mirror back and forth ($\pm\delta\mathrm{u}$) by known amounts in a direction associated with a particular alignment parameter from the current alignment state. We then measure Φ_{A} for each perturbation and subtract one measurement from another. Dividing the result by the total perturbation($2\,\delta\mathrm{u}$) approximates the partial derivative of Φ_{A} at the current alignment state in the direction of the movement. Repeating this for other parameters and replacing Φ_{A} with Z_5, Eq. 2 is converted into,

$$\begin{bmatrix} \partial_{\mathrm{x}_2}\mathrm{Z}_5 \\ \partial_{\mathrm{y}_2}\mathrm{Z}_5 \\ \partial_{\theta_2}\mathrm{Z}_5 \\ \partial_{\phi_2}\mathrm{Z}_5 \end{bmatrix} = \begin{bmatrix} 2\mathrm{L}_{\mathrm{x}_2\,\mathrm{x}_2}, & 0, & 0, & \mathrm{L}_{\mathrm{x}_2\,\phi_2} \\ 0, & 2\mathrm{L}_{\mathrm{y}_2\,\mathrm{y}_2}, & \mathrm{L}_{\mathrm{y}_2\,\theta_2}, & 0 \\ 0, & \mathrm{L}_{\theta_2\,\mathrm{y}_2}, & 2\mathrm{L}_{\theta_2\,\theta_2}, & 0 \\ \mathrm{L}_{\phi_2\,\mathrm{x}_2}, & 0, & 0, & 2\mathrm{L}_{\phi_2\,\phi_2} \end{bmatrix} \begin{bmatrix} \mathrm{dx}_2 \\ \mathrm{dy}_2 \\ \mathrm{d}\theta_2 \\ \mathrm{d}\phi_2 \end{bmatrix} \tag{6}$$

where ∂_{a} is a partial derivative with respect to the parameter 'a'.

In a centred system, the differential wavefront matrix on the right-hand-side of Eq. 6 becomes symmetric because of the alignment influence symmetry [11]. This full-rank matrix has the same number of non-zero singular values as the number of the unknowns. Therefore we can uniquely determine the alignment state by solving the equation. To the second order, Z_5 only allows coupling between two alignment parameters associated with the same pupil axis [11]. Thus we can split the above into two separate equations such that two sets of directional parameters associated with two orthogonal pupil axes can be determined independently. Extending the above to a three-element case, we obtain Eq. 7 used in Section 3.

$$\partial_{\mathrm{u_j}}\mathrm{Z}_5 = \sum_{\mathrm{k}}(1+\delta_{\mathrm{jk}})\,\mathrm{L}^{(2)}_{\mathrm{u_j},\mathrm{u_k}}\,\mathrm{u_k}, \quad \partial_{\mathrm{v_j}}\mathrm{Z}_5 = \sum_{\mathrm{k}}(1+\delta_{\mathrm{jk}})\,\mathrm{L}^{(2)}_{\mathrm{v_j},\mathrm{v_k}}\,\mathrm{v_k} \tag{7}$$

where $\mathbf{u} = (\mathrm{dx}_1, \mathrm{d}\phi_1, \mathrm{dx}_2, \mathrm{d}\phi_2, \mathrm{dx}_3, \mathrm{d}\phi_3)$ and $\mathbf{v} = (\mathrm{dy}_1, \mathrm{d}\theta_1, \mathrm{dy}_2, \mathrm{d}\theta_2, \mathrm{dy}_3, \mathrm{d}\theta_3)$.

#87062 - $15.00 USD Received 30 Aug 2007; revised 24 Oct 2007; accepted 25 Oct 2007; published 6 Nov 2007

2.3. *Effects of measurement and control uncertainties to DWS*

When we have measurement (σ_m) and control (σ_c) uncertainties and perturb a parameter u_i by $\pm\delta u_i$, the wavefront measured N_m times becomes Eq. 8, up to the second order.

$$\Phi(u_i \pm \delta u_i) = \Phi_0 + L^{(1)}_{u_i}\{(u_i \pm \delta u_i) + q(0,\sigma_c)\} + L^{(2)}_{u_i,u_i}\{(u_i \pm \delta u_i) + q(0,\sigma_c)\}^2 + \sum_{j(\neq i)} L^{(2)}_{u_i,u_j}\{(u_i \pm \delta u_i) + q(0,\sigma_c)\}u_j + q(0,\sigma_m/\sqrt{N_m}) \quad (8)$$

where $q(0,\sigma)$ is a Gaussian random variable with zero mean and variance of σ^2, and $L^{(m)}$ is defined in the normalised range of $-1 \le u_i \le 1$. The differential wavefront is then given as,

$$\frac{\partial\Phi}{\partial u_i} = L^{(1)}_{u_i}\left\{1 + \frac{q(0,\sigma_c\sqrt{2})}{2\delta u_i}\right\} + L^{(2)}_{u_i,u_i}\left\{2\left(1 + \frac{q(0,\sigma_c\sqrt{2})}{2\delta u_i}\right)u_i + q(0,\sigma_c\sqrt{2}) + \frac{q^2(0,\sigma_c\sqrt{2})}{2\delta u_i}\right\} + \sum_{j(\neq i)}\left\{L^{(2)}_{u_i,u_j}\left(1 + \frac{q(0,\sigma_c\sqrt{2})}{2\delta u_i}\right)u_j\right\} + \frac{q(0,\sigma_m\sqrt{2/N_m})}{2\delta u_i} \quad (9)$$

As astigmatism associated with $L^{(2)}$ is of interest (Section 2.1), the first order term in Eq. 9 can be neglected. The variance of the differential wavefront, $\sigma^2_{(u_i)}$, can be approximated by Eq. 10.

$$\sigma^2_{(u_i)} \sim \frac{1}{2}\left[(2L^{(2)}_{u_i,u_i})^2\left\{1 + \frac{2u_i}{\delta u_i} + \left(\frac{u_i}{\delta u_i}\right)^2\right\} + \sum_{j(\neq i)}\left\{L^{(2)}_{u_i,u_j}\frac{u_j}{\delta u_i}\right\}^2\right]\sigma_c^2 + \frac{\sigma_m^2}{2N_m\,\delta u_i^2} \quad (10)$$

We notice that several measurements (N_m) can suppress σ_m further while increasing $|\delta u_i|$ seems more effective as $\sigma^2_{(u_i)}$ is inversely proportional to $|\delta u_i|^2$. However, the terms associated with σ_c are independent of N_m and there is one term which is also independent of δu_i, and so limits the lowest possible $\sigma_{(u_i)}$ for a given set of uncertainties. This term remains unchanged even though the alignment state approaches its nominal value ($|u| \to 0$). This control- and measurement-driven uncertainty floor can be expressed as,

$$\lim_{|u|\to 0}\sigma^2_{(u_i)} \sim \frac{1}{2}\left\{(2L^{(2)}_{u_i,u_i})^2\sigma_c^2 + \frac{\sigma_m^2}{N_m\,\delta u_i^2}\right\} \quad (11)$$

2.4. *Effects of surface deformation uncertainty to DWS*

In many systems, especially with large optics, surface deformation is an important uncertainty that can affect the performance of DWS. To see this effect, we use the Zernike polynomials as the characteristic surface deformation elements and then consider their effect to DWS according to the orientation axes of the deformations (Table 1).

Table 1. Classification of surface deformation elements

Classification	Pupil axis	Zernike angular index (l in $Z_{k,l}$)	Effect
G1	ξ	positive odd ($l = +1, +3, +5, \cdots$)	dx, dϕ
G2	η	negative odd ($l = -1, -3, -5, \cdots$)	dy, dθ
G3	z	zeros ($l = 0$)	dz
G4	–	even ($l = \pm 2, \pm 4, \pm 6, \cdots$)	–

G1 and G2 are characterised by their apparent associations with two lateral pupil axes (ξ, η), respectively. These deformation elements change the optical path length and the refraction(or

#87062 - $15.00 USD Received 30 Aug 2007; revised 24 Oct 2007; accepted 25 Oct 2007; published 6 Nov 2007

reflection) angle in a particular direction. This is a very similar behaviour to decentre and tilt of the element in question. We anticipate that such surface deformations would effectively generate additional misalignment in the system of interest, leading to over- or under-estimation of the corresponding directional alignment state.

Deformations of type G3 are associated with the *z*-axis and deform optical surfaces in a rotationally symmetric way. Therefore, the aberrations generated by G3 deformations would be similar to those of the axial misalignment parameters. These could also generate additional misalignment to the parameters and thus affect the state estimation along the optical axis.

G4 deformations have saddle-like patterns characterised by their axes of symmetry. The signs of each symmetric deformation along two adjacent axes are opposite to each other. Thus, we expect that variations in the optical path length and refraction angle would occur without any preferential direction. These deformations can also generate additional misalignments, but the magnitude of these would be too small to influence the alignment state estimation. However, if a G4 deformation is somehow strongly coupled with the alignment parameters such that Φ_C in Eq. 1 is non-negligible, then it could influence the alignment state estimation.

The effect from G1 and G2 can be modelled as the additional alignment state uncertainty (σ_{d}) multiplied by a constant ($\mathrm{C}_{\mathrm{u_i}}$) associated with $\mathrm{u_i}$. This slightly modifies Eq. 11, including the higher-order contributions (σ_{n}) previously ignored in Eq. 2, as,

$$\lim_{|\mathrm{u}|\to 0}\sigma^2_{(\mathrm{u_i})} \sim \frac{1}{2}\left\{(2\mathrm{L}^{(2)}_{\mathrm{u_i},\mathrm{u_i}})^2\sigma_{\mathrm{c}}^2 + \mathrm{C}^2_{\mathrm{u_i}}\sigma_{\mathrm{d}}^2 + \frac{\sigma_{\mathrm{m}}^2}{\mathrm{N_m}\,\delta\mathrm{u}_{\mathrm{i}}^2}\right\} + \sigma_{\mathrm{n}}^2 \tag{12}$$

The uncertainties in the motion control and G1 and G2 surface deformation effectively define the theoretical accuracy limit of the alignment state estimation by DWS as given in Eq. 13.

$$\mathbf{V} \;=\; \mathbf{P}^{\mathrm{T}}\cdot\mathrm{diag}\{\sigma^2_{(\mathrm{u_i})}\}\cdot\mathbf{P} \tag{13}$$

where **P** is the pseudo-inverse of the differential wavefront matrix and **V** is the covariance matrix of the state estimation. Eq. 13 can be used for computing the state estimation quality such that we determine whether the estimation should be used in the subsequent alignment actions.

3. Case studies and Monte Carlo alignment simulations

3.1. Simulation process

Using the wide-field($\pm$0.8 degrees) three-mirror system of [11], we carried out alignment simulations to test the practical feasibility of DWS. We assumed the collimated test beam at the on-axis field and used a single-path wavefront measurement. The simulation parameters are given in Table 2. We used both DWS and MFWS in Case study 1 and then used only DWS for the other case studies and Monte-Carlo alignment simulations. In representing the directional misalignment, we adopted the complex expression [11] which is,

$$\mathrm{dx} + \mathrm{dy}\,\mathrm{i} \;=\; \mathrm{dL}\cdot\mathrm{e}^{\mathrm{i}\,\mathrm{a}}\;(\mathrm{Linear}),\quad \mathrm{d}\phi + \mathrm{d}\theta\,\mathrm{i} \;=\; \mathrm{dR}\cdot\mathrm{e}^{\mathrm{i}\,\mathrm{b}}\;(\mathrm{Angular}) \tag{14}$$

Hereafter the linear and angular misalignment refer to dL and dR in Eq. 14 respectively.

In the first iteration, we used a two-step procedure where the directional misalignment was first estimated by solving Eq. 7 and then used as a constraint for non-linear estimation of the axial misalignment. In comparison to the higher-order couplings between the directional and axial misalignments, the second-order couplings between the directional misalignments normally give a much greater effect to the resultant alignment-driven astigmatism. Therefore it is possible to estimate the directional misalignment independently from the axial misalignment.

#87062 - $15.00 USD Received 30 Aug 2007; revised 24 Oct 2007; accepted 25 Oct 2007; published 6 Nov 2007

However, the axially symmetric aberrations, like defocus, may contain substantial amounts of field curvature-like aberrations by the couplings between directional misalignments. Therefore it is necessary to constrain those effects in estimating the axial misalignment.

By correcting the axial state in the first iteration we can further reduce the non-linear effects from the coupling between the axial and directional states, thereby improving the accuracy of the subsequent directional state estimation. Note that we defined the axial separation between two elements as the axial alignment parameter.

In the subsequent three iterations, we estimated and corrected the directional misalignment only. This left sufficiently small residual directional misalignment. In the final correction we then repeated the two-step procedure of the first iteration, except that the axial misalignment was corrected only when the RMS value of the axially symmetric aberrations is greater than $\lambda/4$.

Table 2. Alignment simulation input parameters

Symbol	Description	Value	Unit
λ	Test wavelength	632.8	nm
σ_m	Measurement noise	$0.1 \sim 30.0$	nm
$\sigma_{c,L}$	Linear control noise	$0.1 \sim 10.0$	μm
$\sigma_{c,A}$	Angular control noise	$0.1 \sim 10.0$	arcsec
N_m	# of measurements	$1 \sim 100$	times
$\delta \mathrm{u_L}$	Deliberate linear perturbation	$0.25 \sim 1.25$	mm
$\delta \mathrm{u_A}$	Deliberate angular perturbation	$0.05 \sim 0.25$	degree
σ_d	Surface deformation	D1, D2, D3, D4	λ
$\mathrm{P_L}$	Range of linear misalignment	± 5.0	mm
$\mathrm{P_A}$	Range of angular misalignment	± 0.8	degree

Note : The motion control noise is applies to the deliberate perturbation as well as the adjustment. D1 corresponds to the radii of curvature variation of M1, M2, and M3 by $+1mm$, $-0.4mm$, and $-0.5mm$ from the nominal values respectively (Case 3). D2 corresponds to the Zernike surface deformation applied to M1 by $Z_5 = \lambda/4, Z_7 = \lambda/7, Z_8 = \lambda/7$ (Case 4). D3 corresponds to the Zernike surface deformation applied to M1 by $Z_4 = \lambda/4, Z_5 = \lambda/4$ and to M2 by $Z_4 = \lambda/5, Z_5 = \lambda/6$ (Case 5). D4 corresponds to the Zernike surface deformations given to M2, where we vary the magnitude of astigmatic (Z_5) and trefoil (Z_{10}) deformation from $\lambda/100$ to $\lambda/4$ (Monte-Carlo simulation). The tilt misalignment range is set as large as the system field-of-view.

3.2. Case study 1 : Ideal case

For the case study 1 we consider ideal optical components and perfect measurements, leaving alignment errors only. This provides an ideal place where we not only compare DWS to MFWS in terms of alignment accuracy, but also quantify the effect of σ_n(in Eq. 12) to DWS.

In the first comparison (Table 3), M1 was perfectly aligned and we only corrected the alignment parameters of M2 and M3. MFWS searched the system alignment configuration showing the most similar Zernike coefficients of focus, 0-deg astigmatism, 45-deg astigmatism, x-coma, y-coma(Z_4, Z_5, Z_6, Z_7, Z_8) to those measured at 10 different fields, by using the actively damped least-square optimisation method. DWS used $\mathrm{N_m} = 1$, $\delta \mathrm{u_L} = 250\,\mu$m, and $\delta \mathrm{u_A} = 180$ arcsec.

Table 3. Comparison 1 : Misaligned M2 and M3

		MFWS(dx, dy, dz, dθ, dϕ)	DWS(dx, dy, dz, dθ, dϕ)
Initial	M2	(+0.500, -0.700, 0.000, +0.250, +0.450)	(+0.500, -0.700, 0.000, +0.250, +0.450)
state	M3	(+1.500, +0.001, 0.000, -0.005, +0.300)	(+1.500, +0.001, 0.000, -0.005, +0.300)
Final	M2	(+0.326, -0.291, -0.460, +0.094, +0.237)	(+6e-6, +5e-6, +0.023, -7e-8, -8e-8)
state	M3	(+1.862, -4.050, -0.224, +0.387, +0.021)	(+8e-6, +5e-6, +0.044, -4e-8, +1e-7)

Note : dx, dy, and dz are in mm while dθ and dϕ are in degree. Normalised field locations for MFWS (Hx,Hy) = {(0,0),($\pm$1,0),(0,$\pm$1),($\pm$0.5,0),(0,$\pm$0.5), (0.5,0.5)}

After 5 corrections, MFWS was unable to eliminate the initial misalignment of the system, especially the decentre and tilt misalignments whereas DWS rectified the alignment state in a

#87062 - $15.00 USD Received 30 Aug 2007; revised 24 Oct 2007; accepted 25 Oct 2007; published 6 Nov 2007

very efficient way. A particularly interesting aspect is that the degeneracies implicit in MFWS lead to some parameters, i.e. dz of M2 and dy, dz, dθ of M3, being moved away from initial positions that were close to the correct one.

For the second comparison, we misaligned all elements and estimated their alignment states simultaneously. MFWS used 15 field locations while DWS used the same parameters as used in the previous comparison. In Fig. 1, we show the alignment state evolutions by both methods.

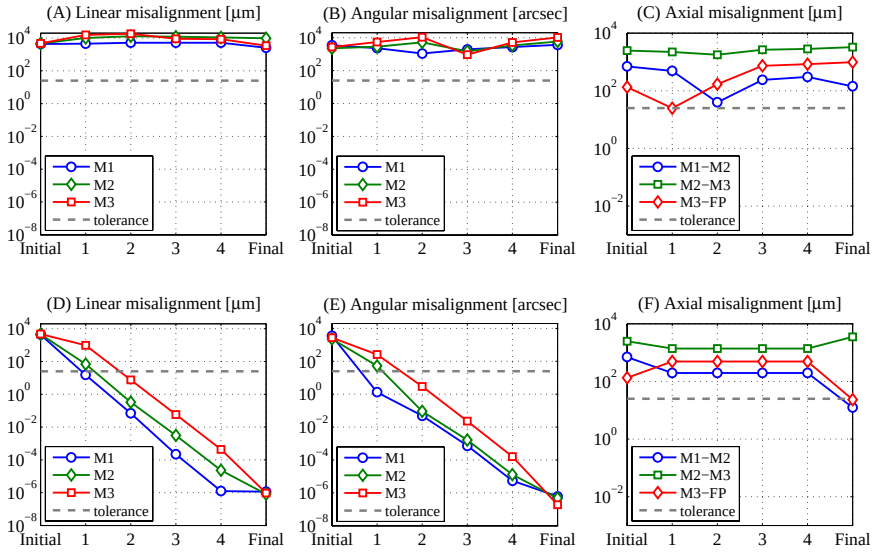

Fig. 1. Alignment state evolutions by MFWS (A-C) and DWS (D-F). Normalised field locations for MFWS (Hx,Hy) = {(0,0),(±1,0),(0,±1),(±0.5,0),(0,±0.5), (±0.5,0.5), (±0.5,-0.5), (+0.25,+0.25), (-0.25,-0.25)}.

No considerable misalignment reduction was made by MFWS (A-C) and the system alignment state after the final correction became very far from the nominal state. DWS showed very contrasting results (D-F). The directional alignment state parameters were corrected to the optically tolerable level after two iterations (D,E). (F) shows that the M1-M2 and M3-FP separations were sufficiently reduced at the final iteration.

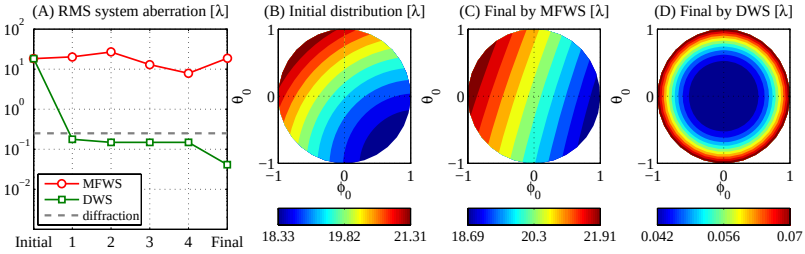

Fig. 2. RMS aberration after corrections by MFWS and DWS.

As a result of these corrections shown in Fig. 1, no considerable suppression by MFWS in the RMS aberration was observed whereas DWS produced substantial reduction by a factor of a few hundreds from the initial value (Fig. 2(A)). The initially tilted field response shown in (B) was not much improved by MFWS (C) while it was recovered to its nominal quadratic shape centred at $(\phi_0, \theta_0) = (0, 0)$ by DWS (D). We note that σ_n in Eq. 12 do not significantly affect the estimation performance of DWS at this level.

#87062 - $15.00 USD Received 30 Aug 2007; revised 24 Oct 2007; accepted 25 Oct 2007; published 6 Nov 2007

3.3. *Case study 2 : Measurement and motion control noise included*

In this case study, we included measurement (σ_m) and motion control (σ_c) uncertainties (Fig. 3). The results show that the directional state estimation reached the correction limit defined by the noise and stagnated after two iterations. The final residual misalignment was also slightly increased relative to Case 1. However, all directional parameters were sufficiently determined and their final misalignments are within tolerance (A,B). The M1-M2 separation reached to its tolerance after one iteration and was further reduced at the final iteration (C). These characteristics were also seen for different initial misalignment ranges, e.g. ± 5 arcmin initial tilt.

The overall performance is reflected in (D) where the minimum and maximum RMS system aberrations over the field are sufficiently suppressed to within the diffraction limit. The initial field response (E) with large variation across the field was corrected to the nearly nominal distribution with small field variation (F). We note that the residual misalignment resulted in the slight offset of the RMS distribution centre from its nominal location.

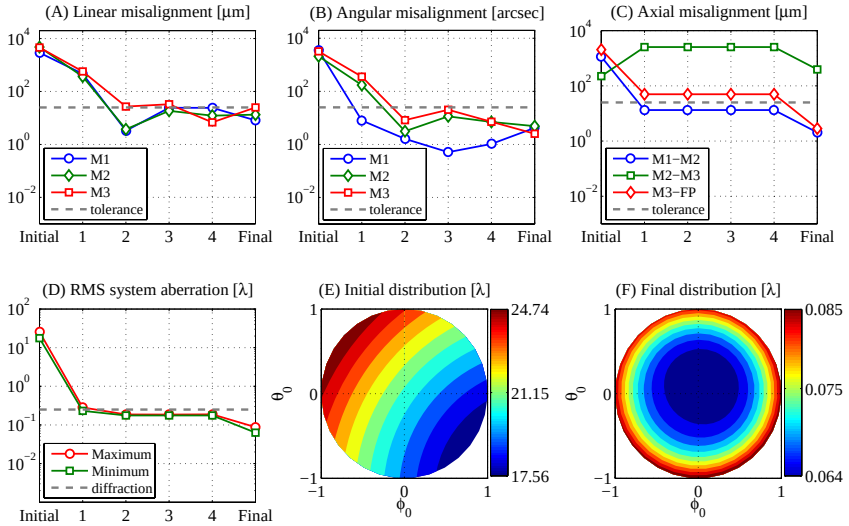

Fig. 3. Case 2 : $N_m = 10$, $\sigma_m = 1.0$nm, $\delta u_L = 250\mu$m, $\delta u_A = 180$arcsec, $\sigma_{c,L} = 1.0\mu$m, $\sigma_{c,A} = 1.0$arcsec

3.4. *Case study 3 : Variation in radii of curvature of M1, M2, and M3*

This type of symmetric surface variation occurs for many reasons in optical systems, e.g. thermal expansion and surface manufacturing error. As the radii of curvature are fundamental parameters contributing to the coefficient matrix in Eq. 7, we can reveal the impact of such a symmetric surface deformation on DWS. Here we changed the radii of curvature of M1, M2, and M3 by $+1mm$, $-0.4mm$, and $-0.5mm$, respectively (Fig. 4). There were also the same amount of measurement and motion control noise employed as in the previous case 2.

The results show that the directional alignment state parameters were well reduced to within the tolerance after two iterations (A,B). The amount of residual directional misalignment also remains at the same level as before, since this is limited by the level of measurement and control noise. It is obvious that the variation in radii of curvature generated additional symmetric aberrations such as defocus, and so the method increased the axial separation between elements to compensate this additional aberration (C,D). As shown previously, the RMS aberration over the field plane also shows a quadratic distribution (F). As we anticipated in Sec. 2.4, this simulation suggests that DWS is insensitive to symmetric surface deformations.

#87062 - $15.00 USD Received 30 Aug 2007; revised 24 Oct 2007; accepted 25 Oct 2007; published 6 Nov 2007

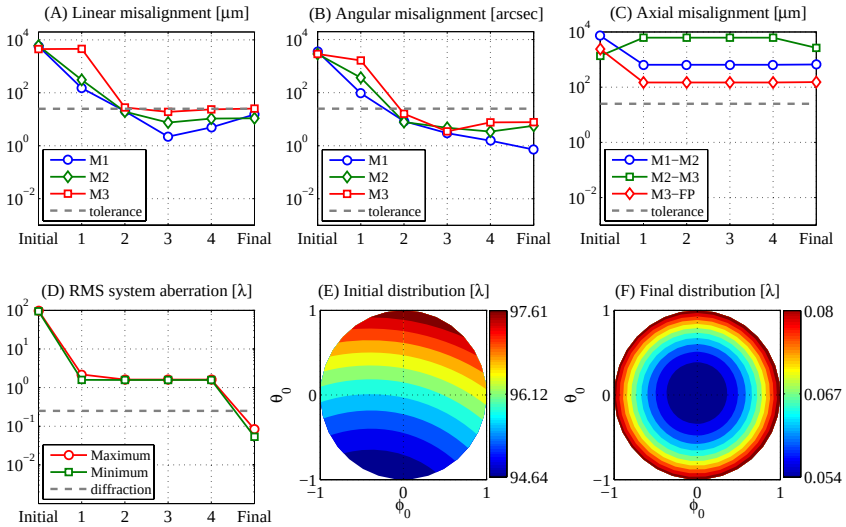

Fig. 4. Case 3 : $N_m = 10$, $\sigma_m = 1.0$nm, $\sigma_d =$ D1(see the note in Table 2), $\delta u_L = 250\mu$m, $\delta u_A = 180$arcsec, $\sigma_{c,L} = 1.0\mu$m, $\sigma_{c,A} = 1.0$arcsec

3.5. *Case study 4 : Astigmatic and comatic surface deformation of M1*

An optical surface can be deformed astigmatically for many reasons. One common reason is residual figure error after surface fabrication. The other is the mounting force by the gravity or other optomechanical stress which can also cause the comatic surface deformation [13]. Investigating the effect of these surface deformations to DWS is, therefore, important. We performed an alignment simulation with astigmatic and comatic surface deformation of M1.

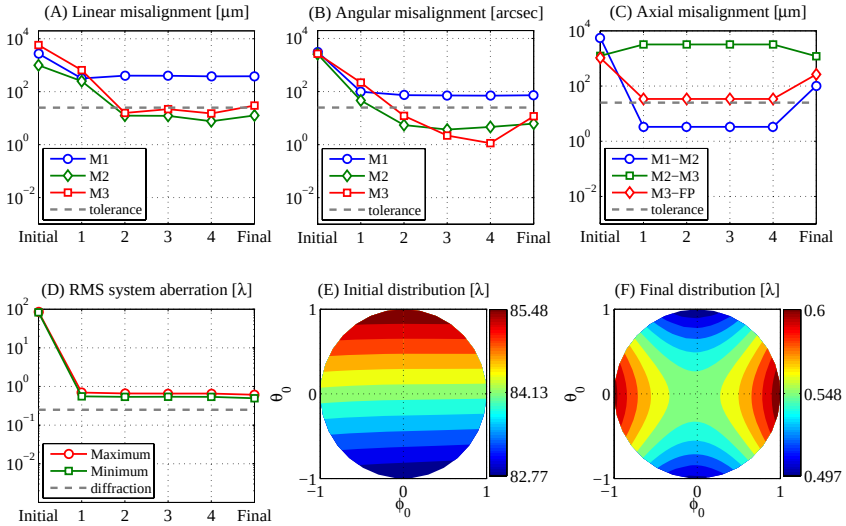

Fig. 5. Case 4 : $N_m = 10$, $\sigma_m = 1.0$nm, $\sigma_d =$ D2(see the note in Table 2), $\delta u_L = 250\mu$m, $\delta u_A = 180$arcsec, $\sigma_{c,L} = 1.0\mu$m, $\sigma_{c,A} = 1.0$arcsec

The results in Fig. 5 show that most of the directional alignment state parameters were brought to within the tolerance limits after the two iterations (A,B). However, M1's linear

#87062 - $15.00 USD Received 30 Aug 2007; revised 24 Oct 2007; accepted 25 Oct 2007; published 6 Nov 2007

and angular misalignment stagnated after the first iteration with relatively large misalignments. This shows that the alignment state estimation and correction can be confused by the comatic or astigmatic surface deformations introduced to M1. Interestingly, only the parameters associated to the deformed surface were over(or under)-estimated while others have been corrected very well regardless of the deformation. This behaviour was also observed when the surface trefoil and astigmatism are present. The surface trefoil belongs to the G1/G2 group and is expected to behave like the surface coma. We will discuss its effects to DWS in more detail in Section 3.7.

The residual directional misalignment generated additional symmetric aberration, which is independent of the axial alignment state. As a result, the axial separations were corrected to minimise this additional wavefront variations (C). The correction left as much aberration as the sum of the surface deformation and the contribution by the residual misalignment (D).

On the other hand, the pattern in Fig. 5(F) becomes similar to *ovals of Cassini* if we extend the field of view further. This pattern has been also reported as a resultant field response due to coupling of field-astigmatism with misalignment [1]. However, in this simulation, the pattern can still be seen in the presence of astigmatic surface deformations, even when the directional alignment state is forced to the correct configuration.

3.6. Case study 5 : Large astigmatic and symmetric surface deformation of M1 and M2

We considered the effect of large symmetric and astigmatic surface deformation to both M1 and M2 with measurement and control noise (Fig. 6).

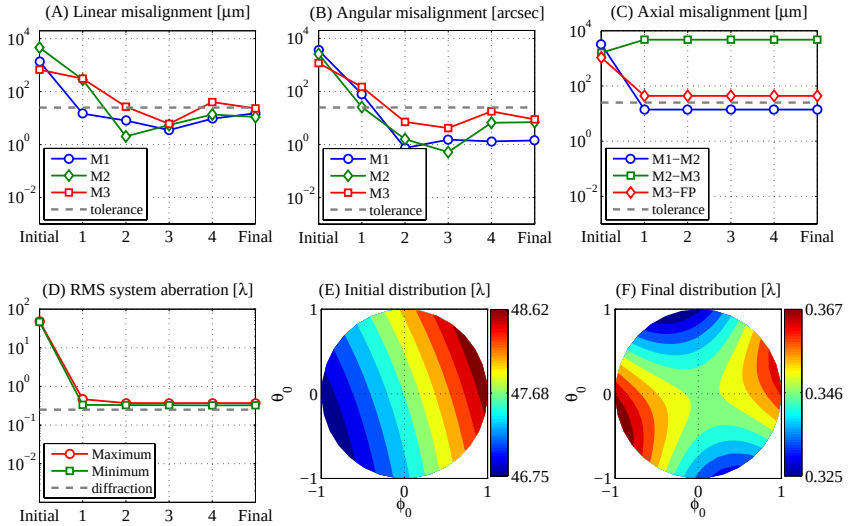

Fig. 6. Case 5 : $N_m = 10$, $\sigma_m = 1.0$nm, $\sigma_d = $D3(see the note in Table 2), $\delta u_L = 250\mu$m, $\delta u_A = 180$arcsec, $\sigma_{c,L} = 1.0\mu$m, $\sigma_{c,A} = 1.0$arcsec

As we have already seen from Fig. 4, the method is insensitive to symmetric surface deformations. Therefore it was expected that the alignment state estimation and correction would not be affected by symmetric deformations in this calculation. On the other hand, the result in Fig. 5 was insufficient to judge which of astigmatic or comatic deformations was actually responsible for the confusion in estimating and correcting the directional alignment parameters. Hence, we carried out this simulation without the comatic deformation.

In Fig. 6(A,B) we see that, despite the presence of large astigmatic and symmetric deformations on M1 and M2, the directional alignment state parameters remain remarkably well

#87062 - $15.00 USD Received 30 Aug 2007; revised 24 Oct 2007; accepted 25 Oct 2007; published 6 Nov 2007

corrected by the method. This is consistent with our expectations from section 2.4, since both the symmetric and astigmatic surface components are independent from the lateral pupil axes.

The axial separations of M1-M2 and M3-FP were sufficiently corrected (C). No further reduction of the system aberration was made after the second iteration because of the surface deformations (D). The initial field distribution showed a large mean value and tilt across the field (E). The alignment correction removed these features although we can still see the strong astigmatic pattern due to the surface deformation (F). This simulation confirms that DWS is insensitive to symmetric and astigmatic surface deformations.

3.7. Monte-Carlo alignment simulation

Finally, we performed Monte Carlo alignment simulations by varying five alignment factors of σ_m, σ_c, δu, N_m, and σ_d. Their representative effects were quantified by the mean values and standard deviations of M2's residual angular misalignment and the RMS system aberration sampled at the field centre.

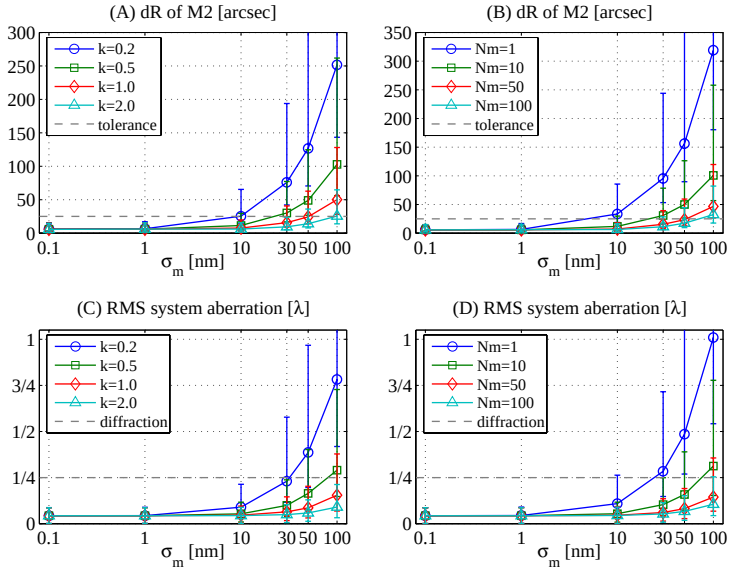

Fig. 7. Monte Carlo alignment simulations : Each point derived from 101 realisations; M2's residual angular misalignment against σ_m with (A) varying k in $\delta u_L = k \cdot 500\mu m$ and $\delta u_A = k \cdot 360$arcsec and (B) varying N_m from its default value of 100. (C,D) are The RMS system aberrations corresponding to (A) and (B) respectively. (Note : $\sigma_{c,L} = 1.0\mu m$, $\sigma_{c,A} = 1.0$arcsec were used. Nm=10 in (A) and k=0.5 in (B). Error bars represent the standard deviations.)

As expected from Eq. 11, the residual misalignment increased as σ_m increased and using large deliberate misalignment (i.e. large k) was certainly helpful in enhancing the final alignment quality (A). However, the effect of the given σ_c to the misalignment is clearly dominant in the region where σ_m is smaller than about 10nm and therefore the curves converge to a non-zero point even at very small σ_m. In (B), the alignment quality improved as we took more measurements, but not as much as the case of increasing the amount of deliberate perturbation as in (A) as described in Eq. 11.

The measurement uncertainty clearly limits the estimation accuracy of DWS. Under controlled environment, one may expect to obtain the measurement uncertainty down to (or often below) few nanometres using stable high-precision interferometers or wavefront sensors.

When the wavefront sensing is exposed to external disturbances, e.g. atmospheric turbulence or vibration, the measurement uncertainty is likely to jump up by a few factors. For example, in

#87062 - $15.00 USD Received 30 Aug 2007; revised 24 Oct 2007; accepted 25 Oct 2007; published 6 Nov 2007

the case of Shack-Hartmann wavefront sensors, the theoretical accuracy under the atmospheric turbulence is about 10nm $\sim$ 30nm in RMS for a given atmospheric coherence length of 10cm at 633nm [14]. However, in some cases, this uncertainty can be increased beyond a few tens of nanometres [15].

These situations are simulated above, showing that the alignment of the example system can be efficiently rectified by DWS and its quality can be even improved by changing two control parameters. This feature can provide a possibility that we can achieve the diffraction limited performance of the system in the alignment test by choosing the two control factors appropriately (C,D). Also, further improvement of the measurement accuracy is feasible when considering the latest wavefront measurement technique [16].

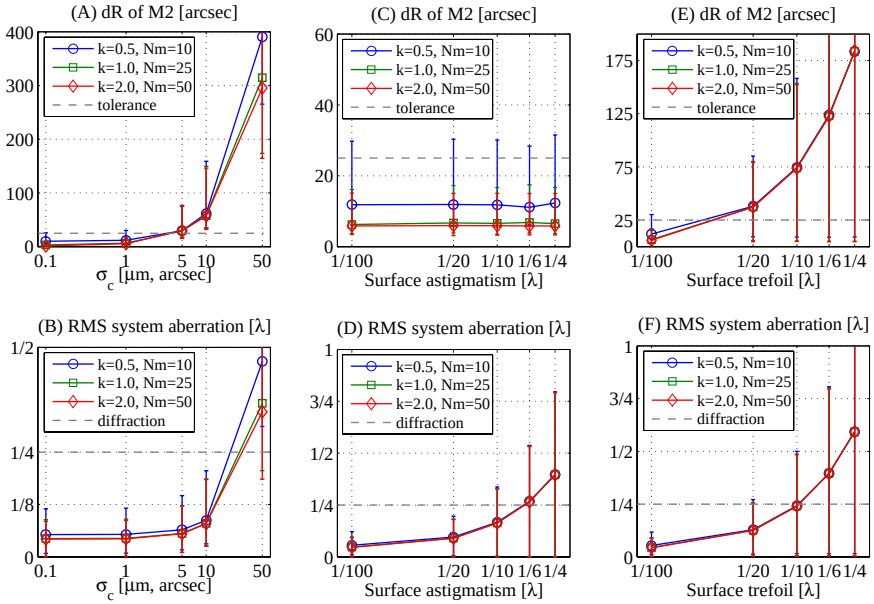

Fig. 8. Monte Carlo alignment simulations : Each point derived from 101 realisations; M2's residual angular misalignment against (A) σ_c, (C) the amount of surface astigmatism, and (E) the amount of surface trefoil. (B,D,F) are the RMS system aberrations corresponding to (A), (C), and (E), respectively. (Note : $\sigma_m = 10$nm, Nm $= 10$ were used in (A). $\sigma_{c,L} = 1.0\mu$m, $\sigma_{c,A} = 1.0$arcsec were used in (C,E). Error bars represent the standard deviations.)

As shown in Fig. 8(A), motion control uncertainty is likely to be critical as it is independent of two control factors and thus unable to be suppressed by them. In particular, precise element movement may not be feasible in some systems. Nevertheless, it is true that precision positioning devices are normally used during the alignment of high-performance systems. In perturbing the elements, DWS only requires relative movement of individual elements. This movement could be precisely controlled using relative position measurements.

In addition, auxiliary information, such as position measurements between elements by other means, can be combined with DWS in order to enhance the alignment quality. In so doing, one can find the acceptable accuracy range of the measurement and motion control device by performing simulations shown above. For this particular example system, the results in (B) suggest that the system can achieve the diffraction-limited performance even though the residual misalignment is higher than the design tolerance. However, to ensure high imaging quality over the field, the RMS control accuracy should be better than about 5μm and 5arcsec while the RMS measurement noise up to 100nm should be acceptable in principle.

#87062 - $15.00 USD Received 30 Aug 2007; revised 24 Oct 2007; accepted 25 Oct 2007; published 6 Nov 2007

On the other hand, the alignment quality was unchanged for different amount of astigmatic surface deformation (C) although the system aberration increased as we put larger amount of surface astigmatism (D). Contrastingly, the alignment quality shows strong dependency on the trefoil deformation, the same kind as the comatic deformation (E). In this case, the system aberration increases more quickly than in the case of (D) as the increased residual misalignment produces additional aberrations. These were anticipated in Table 1 and Fig. 5. Increasing δu and N_m showed no considerable improvement in the final alignment quality in both cases.

It is interesting to discover that surface deformations affect DWS in very different ways depending on the types of deformations, as implied in Table 1. In particular, the deformation patterns investigated in the calculations, i.e. variation in radii of curvature, defocus, astigmatism, coma, and trefoil, frequently appear in either surface fabrication, optics mounting, or both. It should, in principle, be possible to quantify the effect of these to the alignment state estimation and then to adjust the desired alignment tolerance.

Also, the simulations suggests that DWS could be used to estimate the amount of these deformations present in the system. For example, we can estimate the amount of misalignment in the directional parameters and then calculate the expected amount of alignment-driven astigmatism. By subtracting this from the measured astigmatism, we could then quantify the amount of astigmatism due to surface deformations. It would be, however, only possible once the correlation between the G1/G2 surface deformations and the directional misalignment is identified.

Finally, the knowledge of the uncertainties discussed above provide important information on the quality of the alignment state estimation and may have a variety of noise characteristics. Depending on their nature, we can adopt various filtering methods, e.g. Kalman filtering for Gaussian noise [17] and Bayesian filtering for generalised non-Gaussian noise [18], to automate alignment procedures.

4. Conclusion

In this paper, we introduced DWS and discussed its potential in rectifying misalignments of optical systems. By deliberately perturbing optical elements, DWS generates a set of linear equations which is then solved to estimate the alignment state of a system. In comparison to MFWS, DWS showed its superiority in alignment state estimation accuracy. We carried out numerical simulations by varying five key alignment factors, i.e. the measurement and control uncertainties, the amount of deliberate perturbation, the number of wavefront measurements, and surface deformations. They affect the quality of the state estimation in several different ways. It was also found that different classes of surface deformations also affect the estimation differently. Under the presence of these external disturbances, DWS was able to efficiently guide the alignment state of a sample multi-element system toward the nominal state. We conclude that these results illustrate the practical applicability of DWS to centered system alignment experiments.

Acknowledgements

Hanshin Lee gratefully acknowledges the support of the government of the Republic of Korea. The authors thank our colleagues at RAL, Kevin Middleton, Tony Richards, Martin Caldwell, and Marc Ferlet, for useful comments and discussions on this work.

#87062 - $15.00 USD Received 30 Aug 2007; revised 24 Oct 2007; accepted 25 Oct 2007; published 6 Nov 2007